

Experimental study for evaluation of re-wetting velocity on micropillar structures using particle image velocimetry (PIV) technique

Hyeon Taek Nam ^a, Hyunmuk Park ^b, Yoomyeong Lee ^b, Seungro Lee ^{a*}, Donghwi Lee ^{b*}

^aDep. of Mechanical Eng., Jeonbuk National University, 567 Baekje-daero, Deokjin-gu, Jeonju 54896, Korea

^bDiv. of Mechanical System Eng., Jeonbuk National University, 567 Baekje-daero, Deokjin-gu, Jeonju 54896, Korea

*Corresponding authors: seungrol@jbnu.ac.kr (S. Lee), dlee462@jbnu.ac.kr (D. Lee)

1. Introduction

Boiling heat transfer is a crucial candidate for cooling technology due to its high heat transfer efficiency using latent heat absorption [1-3]. Therefore, research on boiling heat transfer is needed for industrial applications such as nuclear power plants that require a large cooling capacity. The main performance of boiling heat transfer is the critical heat flux (CHF) which refers to the maximum heat flux. When the CHF occurs, the heated surface is covered with vapor film (i.e., the insulation layer) owing to the acceleration of bubble merging. Since the vapor film has low thermal conductivity compared to the working fluid (i.e., water), it acts as the insulation layer that prevents heat transfer, resulting in the heated surface's abrupt temperature rise and failure. In this regard, research on CHF enhancement is actively conducted by using micro/nano-structured surfaces due to their high fluid-supply capacity (i.e., wickability).

Wickability represents the performance of liquid flow driven by capillary force on the micro-structured surface. High wickability can promote the fluid supply and delay the formation of vapor film even in high heat flux conditions, resulting in CHF enhancement. The criterion of wicking surface is the critical contact angle, which is defined as follows [4]:

$$\theta_c = \cos^{-1} \frac{1-\phi}{r-\phi} \quad (1)$$

where r is the roughness and ϕ is the solid fraction on the micro-structured surface. When the critical contact angle is larger than the intrinsic contact angle, the wicking phenomena can occur on the surface. Many researchers have suggested CHF prediction models based on the wicking performance of micro/nano-structured surfaces [5-7]. They emphasized that the re-wetting velocity, which acts as fluid supply to the contact line of the bubble, becomes higher with the wicking velocity, enhancing the bubble's detachment and delaying the formation of a vapor film. However, since re-wetting velocity in an actual boiling condition is a function of not only wicking velocity but also bubble-induced re-wetting velocity (i.e., quenching flow), research to evaluate CHF improvement by decoupling these factors is needed.

In this study, we conducted the boiling heat transfer experiment using the micro-pillar structured surface (MPS) and measured the inflow velocity (i.e., re-wetting velocity) near the contact line of the bubble using the particle image velocimetry (PIV) technique. Next, we demonstrate the CHF enhancement factor (e.g., wicking

and quenching flow) of the MPS samples by using the analyzed PIV images.

2. Methods and Results

2.1 MPS sample fabrications

We fabricated the MPS samples using the micro-electro-mechanical systems (MEMS) process. Before the fabrication, the P-type silicon wafer (orientation of 100, resistivity of 1–10 Ω) was cleaned with piranha and buffered oxide etchant (BOE) solution to remove the organic materials and oxidation layer, respectively. The cleaned wafer was coated with a positive photoresist (PR). After the UV lithography, the coated PR was left with only a micro-dot array. The deep reactive-ion etching (DRIE) process was conducted to make the micro-pillar structured surface. During the DRIE process, a polymeric passivation layer was used to prevent over-etching of the pillar sidewall. After the DRIE process, the remaining PR and the passivation layer were removed by the Asher process. The micropillar had a height (H) of 15 μm , a diameter (D) of 4, 10, or 20 μm , and a gap (G) between the micropillars of 10 or 20 μm . Table 1 and Figure 1 show the geometric variables and schematic diagrams of MPS samples, respectively.

2.2 Experimental setup

Figure 2 shows the experimental schematics for boiling tests and PIV measurements. The boiling experiment consists of a water pool, DC power supply, copper (Cu) block heater, and data acquisition equipment.

The water pool has a capacity of 7.0 L, and DI water was used as the working fluid for the pool boiling experiment. To remove the dissolved oxygen in the DI water, we conducted the degassing process for at least 1 hour before the boiling test. The Cu block heater was used to supply heat to the MPS samples. Using the DC power supply (Asterion DC, ~3.3kW), we supplied the heat to the four DC cartridge heaters (48V, 100W) inserted in the Cu block. For the reduction of thermal contact resistance, the thermal greases, which have a thermal conductivity of 12.5 W/mK, were applied between the Cu block and the MPS sample. To measure the temperature, we mounted four k-type thermocouples in the Cu block along a vertical direction and used a data logger (Agilent 34970A). All temperature data were measured at a steady state.

Table 1 Geometric variables of MPS samples

	D (um)	G (um)	H (um)	r	ϕ
Plain surface	-	-	-	1	-
D04 G10	04	10	15	2.51	0.064
D04 G20	04	20	15	1.51	0.022
D10 G20	10	20	15	1.82	0.087
D20 G20	20	20	15	1.93	0.196

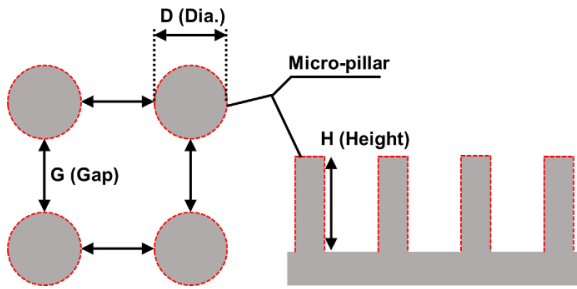


Fig. 1 Schematic diagrams of the micropillar structured surface.

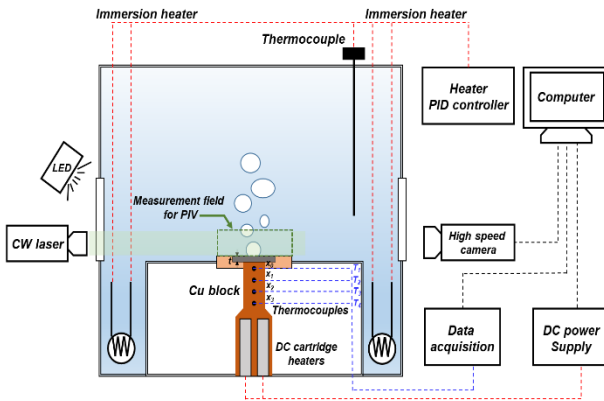


Fig. 2 Experimental apparatus of pool boiling heat transfer system.

For PIV measurement, we used the LED ramp, a continuous (CW) laser (Ray Power, 5W, wavelength of 532nm), and a high-speed camera (Photron, SA3, 2000fps). The fluorescent polymer particles for PIV were used to visualize the flow around the bubble. When the particle receives the laser beam (~532 nm), the emitted light from the particle has a wavelength of 600 nm. To block the scattered light (~532 nm) from the bubble by the laser beam and visualize only the light (~600 nm) emitted by the particles, we mounted a 600 nm band-pass filter on the high-speed camera. We used the software (Dynamic studio) for PIV analysis, and PIV images were recorded at 2000 Hz.

2.3 PIV results: re-wetting velocity

Figure 3 (a) and (b) show the PIV images of the plain surface and D04 G10 sample at the heat flux of 90 W/cm², respectively, where the CHF occurs on the Plain surface. In the case of the plain surface, the bubble merging actively occurred, and vapor film covered the heated surface. In contrast, the D04 G10 having the highest wicking performance in the previous study [8], shows the bubble detachment still appears well. For the velocity contour around the bubble, D04 G10 shows a strong re-wetting flow to the contact line of the bubble compared to the measured flow at the plain surface.

Figure 3 (c) shows the distribution of x-direction velocities along the 5 mm length from the bubble. As seen in the graph, it is confirmed that the large re-wetting velocity to the contact line of the bubble is distributed broader region on the D04 G10 sample. We inferred that the high re-wetting velocity on the D04 G10 sample is due to the high wicking performance. The high wicking velocity can promote the re-wetting velocity on the heated surface by the capillary force. Additionally, the large wicking performance can delay the bubble merging, even in high-heat flux conditions, enhancing the re-wetting flow.

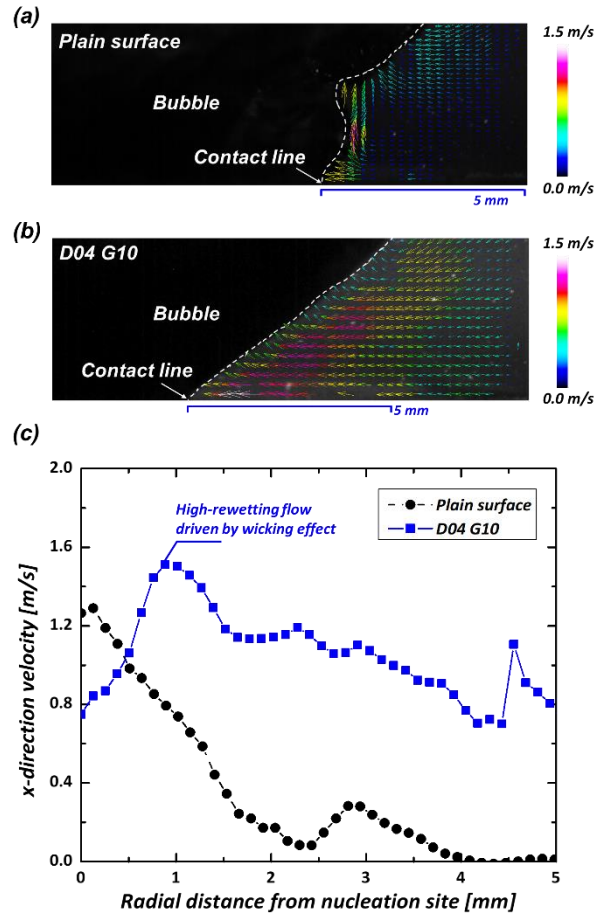


Fig. 3 (a) PIV images on the plain surface, (b) PIV images on the D04 G10 MPS sample, and (c) the comparison of re-wetting velocity along the 5 mm length from the bubble

3. Conclusions

In this study, we measured the re-wetting velocity on the MPS samples using the PIV technique to clarify the CHF enhancement by wickability of microstructures. As a result, the wickability significantly contributed to enhancing the re-wetting flow into the contact line of bubbles. Based on these findings, further research will aim to decouple the bubble-induced flow and wicking flow, which are consisting the re-wetting velocity. Then, these results will be used as data to validate the simulation results of the CHF enhancement.

Acknowledgement

This work was partly supported by the National Research Foundation of Korea(NRF) grant funded by the Korea government(MSIT) (No. RS-2022-00166991) and by the Basic Science Research Program through the NRF funded by the Ministry of Education (Grant Number: NRF-2021R1I1A3052326).

REFERENCES

- [1] D. Lee, N. Lee, D.I. Shim, B.S. Kim, and H.H. Cho, Enhancing thermal stability and uniformity in boiling heat transfer using micro-nano hybrid surfaces (MNHS), *Applied Thermal Engineering*, 130, pp. 710-721, 2018.
- [2] D.E. Kim, D.I. Yu, D.W. Jerng, M.H. Kim, and H.S. Ahn, Review of boiling heat transfer enhancement on micro/nanostructured surfaces, *Exp Therm Fluid Sci*, 66, pp. 173-196, 2015.
- [3] S. Ridwan, J. Pollack, and M. McCarthy, Nanofluid Boiling on Micro/Nano-engineered Surfaces, *Langmuir*, 37(20), pp. 6107-6114, 2021.
- [4] D.I. Shim, G. Choi, N. Lee, T. Kim, B.S. Kim, and H.H. Cho, Enhancement of Pool Boiling Heat Transfer Using Aligned Silicon Nanowire Arrays, *ACS Appl Mater Interfaces*, 9(20), pp. 17595-17602, 2017.
- [5] H.S. Ahn, G. Park, J.M. Kim, J. Kim, and M.H. Kim, The effect of water absorption on critical heat flux enhancement during pool boiling, *Exp Therm Fluid Sci*, 42, pp. 187-195, 2012.
- [6] Y. Song, C. Wang, D.J. Preston, G. Su, M.M. Rahman, H. Cha, J.H. Seong, B. Philips, M. Bucci, and E.N. Wang, Enhancement of Boiling with Scalable Sandblasted Surfaces, *ACS Appl Mater Interfaces*, 14(7), pp. 9788-9794, 2022.
- [7] M.M. Rahman, E. Olceroglu, and M. McCarthy, Role of wickability on the critical heat flux of structured superhydrophilic surfaces, *Langmuir*, 30(37), pp. 11225-11234, 2014.
- [8] H.T. Nam, D. Lee, and S. Lee, Experimental study of the pool boiling heat transfer characteristics on micro-pillar structured surfaces with various wickability, *Korean Society of Mechanical Engineers*, Nov. 9-12, 2022, Jeju, Korea